CIRP Journal of Manufacturing Science and Technology xxx (2019) xxx–xxx

Contents lists available at ScienceDirect

CIRP Journal of Manufacturing Science and Technology

journal homepage: www.elsevier.com/locate/cirpj

Evaluating tool point dynamics using output-only modal analysis with mass-change methods

Pulkit Gupta[a], Mohit Law[a,*], Suparno Mukhopadhyay[b]

[a] Machine Tool Dynamics Laboratory, Department of Mechanical Engineering, Indian Institute of Technology Kanpur, Kanpur 208016, India
[b] Department of Civil Engineering, Indian Institute of Technology Kanpur, Kanpur 208016, India

ARTICLE INFO

Article history:
Available online xxx

Keywords:
Dynamics
Cutting tool
Output-only modal analysis
Mass-change
FRFs

ABSTRACT

This paper discusses the evaluation of tool point dynamics using output-only modal analysis methods. As compared to the traditional experimental modal analysis procedures that rely on the input and the output, both being known, output-only methods discussed herein can evaluate modal parameters using only the measured response of the tool subjected to unknown impact-based excitations. Since the input is not known, the estimated shapes are unscaled. To correctly scale shapes, we use the mass-change method. We present analytical models to guide the optimal selection of the mass to be added as well as to guide its placement on the tool. Analytical models systematically characterize errors in scaling the eigenvector and errors due to uncertainties in the estimation of the natural frequencies. The model suggests placement of the mass to be added at the anti-node(s) for the mode(s) of interest. These models guide experiments on two tools – a slender boring bar, and an end mill. Tool point frequency response functions (FRFs) reconstructed with the natural frequencies, damping ratios, and scaled mode shapes evaluated with the output-only mass-change method are compared with and found to be in good agreement with FRFs obtained from the traditional experimental modal analysis procedures. Since output-only methods require one less transducer, and since these methods are robust to uncertainties and inconsistencies in the input, output-only methods promise advantages from the industrial point of view.

Introduction

High-performance machining capabilities are governed by tool point dynamics. These dynamics are generally characterized by measured frequency response functions (FRFs). Measured dynamics serve as inputs to machining stability models that guide the selection of cutting parameters to ensure high-productivity chatter-free machining [1,2]. Uncertainties in the measured dynamics are one of the main sources of errors in the predicted stability [3]. There is hence a great deal of emphasis on correctly measuring the FRFs.

Tool point FRFs are generally measured by exciting the tool tip using an impact hammer instrumented with a load cell. Response to this excitation is usually measured using accelerometers mounted on the tool tip or by using other non-contact sensors such as laser vibrometers. The spectra of the output response divided by the input force results in the FRF. These FRFs can directly be used in frequency-domain stability models, or modal parameters can be extracted from the measured FRFs using one of the many modal parameter estimation algorithms [4] for use in time-domain stability models. Though these impact-based experimental modal analysis (EMA) procedures have become routine to estimate tool point dynamics, EMA sometimes poses difficulties.

Because impacts are applied manually, it is challenging to apply the same input force consistently. This can make the measurement non-repeatable. Furthermore, since machines are weakly nonlinear, a higher/lower force input may result in slight variations in the measured FRFs. The bandwidth of excitation also depends on the choice of the hammer's tip. Using harder tips for higher frequency excitation many-a-times results in multiple hits. Using softer tips does not excite the tool and results in bad data quality. This makes the measurement to be dependent on the operator's skill and experience – especially so for measuring very flexible tooling systems. Some of the above issues can be addressed by using an instrumented modal shaker to excite the tool. However, stinger-shaker-tool interaction poses its own set of challenges [4], and it is difficult to decouple the response of stinger and the shaker from the tool.

* Corresponding author.
E-mail address: mlaw@iitk.ac.in (M. Law).

https://doi.org/10.1016/j.cirpj.2020.06.001
1755-5817/© 2020 CIRP.

This paper addresses some of the above articulated challenges by using an output-only modal analysis method to estimate tool point dynamics. Output-only modal analysis is part of the family of the operational modal analysis (OMA) procedures. OMA is routinely used in civil structural engineering applications [5], wherein it is not always possible to measure random excitation that those structures are subjected to, but it is still of interest to estimate the structure's modal parameters during operating conditions using output-only response data. In a similar vein, this paper discusses the estimation of tool point dynamics using output-only data without having to measure the input force signals. Output-only methods discussed in this paper rely less on the operator's skill of measurement and are more robust to non-repeatability issues during measurements as well as being more robust to multiple hits during excitation. Since the proposed methods require one less transducer, they promise advantages from the industrial point of view.

Operational modal analysis procedures have already gained traction in the evaluation of the dynamics of machine tool systems [6–32]. Since traditional EMA procedures obtain tool point FRFs at zero speeds and for when the tool is not contacting the workpiece, the main motivation for using OMA in the context of machine tools has been to evaluate how the dynamics of machines change with speed and, a change in contact conditions between the tool and the workpiece during cutting.

Evaluation of the machine's dynamics in the operational state has been shown possible by measuring the response of non-rotating components during cutting process-based excitation. Some of the OMA implementations measured cutting forces using a dynamometer and used those in reconstructing the FRFs [6–12]. However, since dynamometers generally have limited bandwidths, higher frequency tool point FRFs are difficult to estimate using these methods. Other OMA approaches in machine tools relied on simulated forces in conjunction with response measured under cutting force-based excitation [13], or on hybrid methods in which forces were measured from EMA and response was measured during OMA [14]. Another method to estimate the speed dependent operational dynamics involved performing impact tests on a rotating tool and using non-contact measurements followed by EMA [15]. Such methods are however fraught with risks. All these [6–15] methods use input forces in estimating dynamics in the operational state, and hence are not strictly based on the output-only analysis.

Some other implementations of OMA in machines do not measure the input forces during cutting-process based excitation [16–22], nor do they measure input forces based on exciting the machine by rapid and sudden changes in the table motion [23,24]. Since the input is not measured in these approaches [16–24], the eigenvectors that are estimated are unscaled, and cannot be used to reconstruct tool point FRFs – which are required for stability predictions. Other operational procedures based on the 'inverse stability analysis' methods [15,25–27] that also do not measure the input force have been reported as capable of identifying the modal parameters using optimization and regression models. However, these methods require extensive experimentation at unstable conditions, and hence are prohibitive. Recent findings concerned with estimating stability margins in turning reported in [28] discussed the identification of modal frequencies and damping using classical OMA procedures without however discussing the estimation of the eigenvectors. Yet other implementations of OMA procedures in the machine tool domain were concerned with the identification of process damping coefficients in orthogonal cutting [29] and in milling [30], without being concerned with estimating modal parameters to reconstruct tool point FRFs, which forms the focus of this paper.

Of all the OMA implementations in machine tools, except for the interesting method proposed in [31] that relies on scaling the eigenvectors using a change in dynamics due to position, or the output-only modal analysis method proposed in [32] that uses the method of mass-change to scale the eigenvectors for micromilling tooling systems, no other OMA based approach that does not measure forces has suggested ways of scaling the FRFs. However, since stability predictions necessitate the use of mass-normalized eigenvectors to reconstruct the tool point FRFs, the output-only methods that do not offer ways of scaling the FRFs are of little use in machining stability predictions. Since this paper is concerned with evaluating tool point FRFs using output-only modal analysis methods which result in unscaled eigenvectors, we also address estimating scaling factors for the eigenvectors to estimate tool point FRFs correctly.

Scaling is a classical problem in OMA and has hence received much attention [33–38]. It has been shown that by making local changes in the mass distribution of the structure such that there is a discernible change in the natural frequencies and no perceptible change in the shapes, scaling factors can be obtained from the measured shift in natural frequencies between the original and the modified condition [33,34]. This paper also adopts such a mass-change method to estimate the scaled eigenvector.

Determining the proper amount of mass(es) to be added and figuring where to place the mass(es) such as to guarantee a perceptible shift in natural frequencies while not changing the shape is non-trivial – and has been limitedly addressed by some researchers [37–40]. However, earlier efforts at determining the correct scaling factors were more focused on placing multiple masses on the structure, such as to obtain the complete mode shape – as was required for those applications. However, in the context of determining only the tool point FRFs – as are targeted in this contribution, we only require the scaled eigenvector at the tool point. We hence reformulate the mass-change method to obtain the scaling factor by placing only a single locally distributed mass at an optimal location on the tool. We present an analytical-based approach to determine *what* amount of mass is to be placed *where* to minimize the error in the scaled eigenvector. This is indeed the key technical contribution of this paper.

This paper demonstrates the reconstruction of tool point FRFs by using output-only response analysis with the mass-change method for two representative tools. One tool is a slender boring bar mounted in a compression holder on a CNC lathe, and another is an end mill mounted in a regular holder on a medium-sized three-axis CNC milling machine. All analysis presented in this paper is for non-rotating tools, i.e., for the case of zero speeds and for the case of the tool not in contact with the workpiece. Furthermore, all analysis presented herein is limited to the case of all modes identified being very well separated.

To extract the modal parameters of interest from the measured output-only time-series data, of the many available identification methods [4], we prefer to use the classical and robust time-domain Eigensystem Realization Algorithm [41]. We hence obtain the natural frequencies, damping ratios, and unscaled mode shapes. An overview of this method is presented in the section on output-only modal analysis using the Eigensystem Realization Algorithm. This is followed by the section on the scaling of shapes using mass-change methods. Since cutting tools are essentially cantilevered, we model the tools as Euler–Bernoulli cantilevered beams, and use these analytical models to find the optimal size and placement location of the mass to be added. Since the added mass is distributed and not a point or a two-point mass, as has been customarily assumed [37–40], we present systematic error analysis of the scaled shape to the method of lumping and/or distributing the mass which is more representative of the real case. We also address the sensitivity of the scaling factors to errors in the

Please cite this article in press as: P. Gupta, et al., Evaluating tool point dynamics using output-only modal analysis with mass-change methods, NULL (2020), https://doi.org/10.1016/j.cirpj.2020.06.001

estimation of the natural frequencies. This is followed by a section presenting the experimental validation of these proposed methods by discussing four ways to add mass on a cantilevered rod. Learnings guide the output-only experimental analysis for tool point FRF reconstruction. An overview of the procedures adopted in this paper is outlined in Fig. 1.

The final main section on the evaluation of tool point dynamics demonstrates the efficacy of the proposed methods on the two tools. Reconstructed FRFs using the proposed output-only mass-change methods are contrasted in that section with FRFs obtained using the classical experimental modal analysis procedures in which the input is known. This is followed by the main conclusions of the paper, which includes discussions on the limitations of the proposed approach.

Output-only modal analysis using the Eigensystem Realization Algorithm

This section outlines the procedure to estimate the natural frequencies, the damping ratios, and the unscaled mode shapes from the measured time response of the system using the Eigensystem Realization Algorithm (ERA). We prefer ERA over other output-only modal analysis methods due to its robustness, and since ERA works well with free decay responses – which is what we have for tools subjected to impulse type excitations, even when the inputs remain unmeasured. Though ERA procedures usually identify a minimum order state space model of a system from the unit impulse response (Markov parameters) of the system, since inputs in the present case remain unmeasured, the measured output will be a scaled version of the system Markov parameters (with unknown scaling), similar to the auto-correlation function of the output for random and white input [5]. Hence, the measured output in the present case can be directly used in ERA to get the unscaled system modes. Key steps of the ERA are presented below, and for additional details, the reader is directed to [41].

Let the discrete time response to an impulse input measured with an accelerometer be written as given in Eq. (1):

$$y = \{y[0], \ldots, y[n-1]\}, \tag{1}$$

wherein n are the number of data points. This response is used to construct a Hankel matrix, $\mathbf{H}_0$ of size, $p \times p$ as given in Eq. (2):

$$\mathbf{H}_0 = \begin{bmatrix} y[0] & y[1] & \cdots \\ y[1] & y[2] & \cdots \\ \vdots & \vdots & \ddots \end{bmatrix}_{p\times p}. \tag{2}$$

A singular value decomposition (svd) of $\mathbf{H}_0$ is then carried out as:

$$\text{svd}(\mathbf{H}_0) = \mathbf{USV}^{\mathrm{T}}. \tag{3}$$

This results in two unitary matrices, **U** and **V,** and a non-negative diagonal matrix, **S** consisting of singular values of $\mathbf{H}_0$ as shown in Eq. (3). The resulting **U**, **S** and **V** matrices are subsequently reordered and truncated based on the number of non-zero singular values in **S**. The reordered and truncated matrices, $\mathbf{U}_1$, $\mathbf{S}_1$ and $\mathbf{V}_1$ are used to construct a truncated observability matrix given by:

$$\Theta = \mathbf{U}_1\mathbf{S}_1^{1/2}, \tag{4}$$

where from the first row of Θ gives the output matrix:

$$\tilde{\mathbf{c}}_d = \Theta(1,:). \tag{5}$$

The observability matrix and a shifted Hankel matrix, $\mathbf{H}_1$:

$$\mathbf{H}_1 = \begin{bmatrix} y[1] & y[2] & \cdots \\ y[2] & y[3] & \cdots \\ \vdots & \vdots & \ddots \end{bmatrix}_{p\times p}, \tag{6}$$

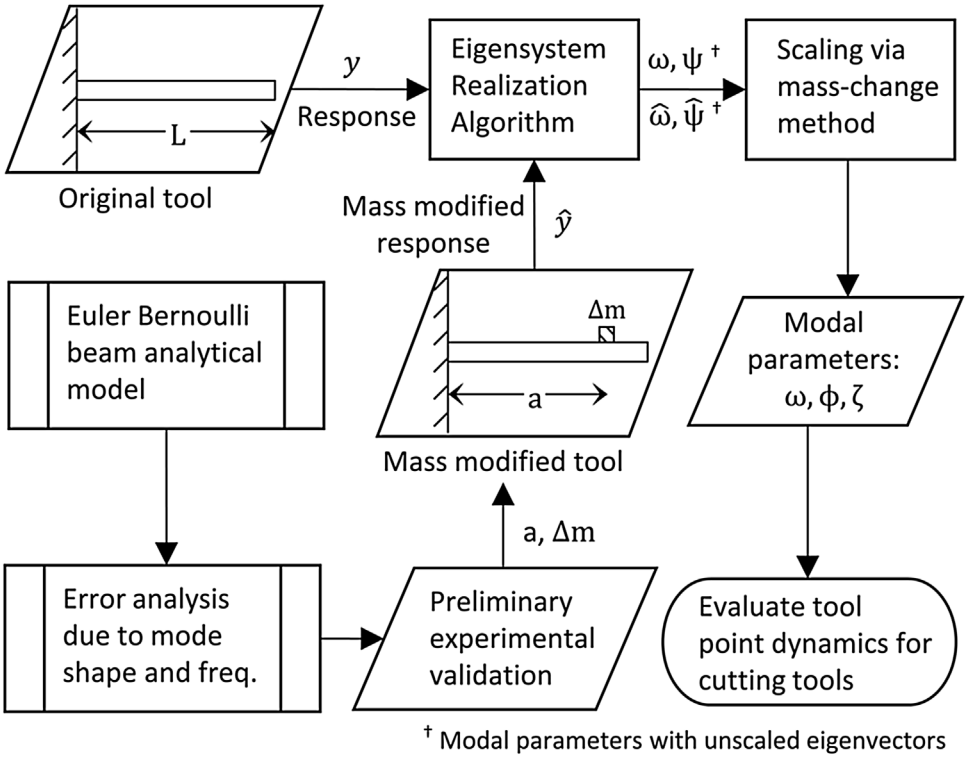

Fig. 1. Overview of the key procedures to obtain tool point dynamics using output-only mass-change methods.

Please cite this article in press as: P. Gupta, et al., Evaluating tool point dynamics using output-only modal analysis with mass-change methods, NULL (2020), https://doi.org/10.1016/j.cirpj.2020.06.001

are then together used to obtain a discrete-time state transition matrix, $\tilde{\mathbf{A}}_d$ as given by Eq. (7):

$$\tilde{\mathbf{A}}_d = \Theta^{+}\mathbf{H}_1\Theta = \mathbf{S}_1^{-1/2}\mathbf{U}_1^{\mathrm{T}}\mathbf{H}_1\mathbf{V}_1\mathbf{S}_1^{-1/2}, \tag{7}$$

where '+' denotes pseudo inverse of the observability matrix.

Eigenvalue analysis of this discrete-time system matrix results in discrete-time complex eigenvalues ($\mathbf{\Lambda}_\mathrm{d}$) and eigenvectors ($\mathbf{\Psi}_\mathrm{d}$) which can, in turn, be converted to continuous-time eigenvalues and eigenvectors as given by Eq. (8):

$$\lambda_j = \frac{1}{\Delta t}[\ln|\Lambda_{dj}| + i\theta_j], \quad \psi_c = \tilde{\mathbf{c}}_d\Psi_d, \tag{8}$$

wherein, $\tilde{\mathbf{c}}_d$ is evaluated from Eq. (5), $\Lambda_{dj} = jth\ \Lambda_d$ and θ_j= argument of $j\mathrm{th}\Lambda_d$, and ψ_c is the complex valued unscaled eigenvector. The real valued unscaled eigenvector, ψ is obtained from ψ_c by minimizing the imaginary part of the corresponding identified complex ψ_c [42]. From λ_j, the jth natural frequency can be evaluated as: $\omega_j = |\lambda_j|$, and the jth modal damping ratio, in turn, can be evaluated to be: $\zeta_j = -\mathrm{Re}(\lambda_j)/\omega_j$.

An overview of the ERA to obtain the modal parameters of interest from the measured response is summarized in Fig. 2. Since the eigenvectors remain unscaled, the methods to scale these correctly such as to obtain the tool point FRFs are discussed next.

Scaling using the mass-change method

In general, the mass-change method involves adding a known mass to the system such that the mode shape of the system remains relatively unaffected even with a notable frequency shift [33,37]. To demonstrate the central idea of the mass-change method, consider the eigenvalue problem associated with a spring-mass system, as shown in Eq. (9):

$$\mathbf{M}\psi\omega^2 = \mathbf{K}\psi, \tag{9}$$

wherein, $\mathbf{M}$ and $\mathbf{K}$ are mass and stiffness matrices, respectively, ψ is the unscaled mode shape, and ω represents the natural frequency of the original system, i.e., before the addition of any mass. On adding a mass of $\Delta\mathbf{M}$, the eigenvalue problem for the modified system becomes:

$$(\mathbf{M} + \Delta\mathbf{M})\hat{\psi}\hat{\omega}^2 = \mathbf{K}\hat{\psi}, \tag{10}$$

wherein, $\hat{}$ represents modal parameters of the new system after adding the mass. This mass addition to the system can be thought to be a form of a structural dynamic modification strategy.

If the mode shapes before and after the mass addition remain the same, i.e., $\psi \cong \hat{\psi}$, Eqs. (9) and (10) can be combined to result in:

$$\mathbf{M}\psi\left(\omega^2 - \hat{\omega}^2\right) = \Delta\mathbf{M}\psi\hat{\omega}^2. \tag{11}$$

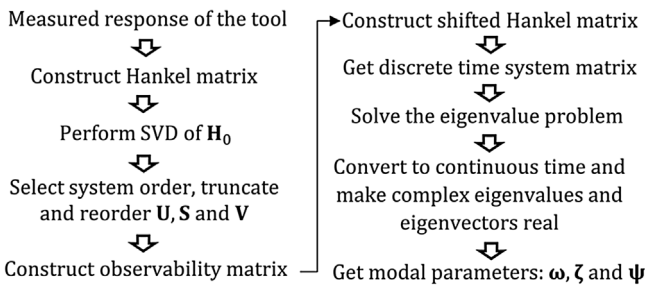

Fig. 2. Overview of the Eigensystem Realization Algorithm to obtain the modal parameters of interest.

For mass normalizing shapes, it is of our interest to obtain a scaling factor, α, such that the mass normalized mode shape, $\phi = \alpha\psi$ satisfy the orthogonality condition $\phi^T\mathbf{M}\phi = \mathbf{I}$. Rewriting Eq. (11) after pre-multiplying it by ψ^{T} results in:

$$\alpha^2 = \frac{\omega^2 - \hat{\omega}^2}{\hat{\omega}^2}\left(\psi^T\Delta\mathbf{M}\psi\right). \tag{12}$$

Though Eq. (12) is straightforward, determining *how* much mass to add *where* on the system remains elusive. These questions will be addressed in the subsequent section through an analytical treatment of a beam model that will guide the sizing and placement of the mass to be added on the tool to scale the shape correctly.

Optimizing size and location of the mass-change using analytical beam formulations

Since this paper is only concerned with evaluating cutting tool point dynamics, and cutting tools are all cantilevered, we propose an analytical model based on the Euler Bernoulli beam theory to optimally size and locate a mass on the tool. Moreover, since we are interested only in the tool point dynamics, and not the entire mode shape of the tool, we limit ourselves to determining where the optimally sized single mass must be placed on the tool so as to reconstruct the scaled eigenvector only at the tool point. The analysis presented below is hence tailored to the application of interest and does not address the generalized question of placing multiple masses at multiple locations so as to obtain the complete shape of the structure of interest – as has been limitedly addressed by others before [34–38].

Euler Bernoulli beam formulation

The three beams for which analytical models are presented herein are shown schematically in Fig. 3. The cases include a simple beam without a mass, a beam with a point mass added at some location, 'a' from the clamped end, and a beam with a distributed mass added over some width, 'd' at some location 'a', measured from the clamped end to the centre of distributed mass.

Since tools are usually slender, the Euler Bernoulli beam model for the tool is thought to be more appropriate than the Timoshenko beam model. The governing equation of motion of an undamped Euler Bernoulli cantilevered beam without any additional mass on it can be shown to be [43]:

$$\rho A\frac{\delta^2 w}{\delta t^2} + EI\frac{\delta^4 w}{\delta x^4} = 0, \quad \begin{cases} w(0) = 0 \\ w'(0) = 0 \\ w''(L) = 0 \\ w'''(L) = 0 \end{cases}, \tag{13}$$

wherein, w is the deflection of the beam, ρ is the density of the material, A is the cross-sectional area, E is the elastic modulus, I is the area moment of inertia of the cantilever beam, and "'" denotes derivative with respect to "x". Eq. (13) also lists the boundary conditions, i.e., the deflection and slope are zero at the clamped end, whereas bending moment and shear force are zero at the free end.

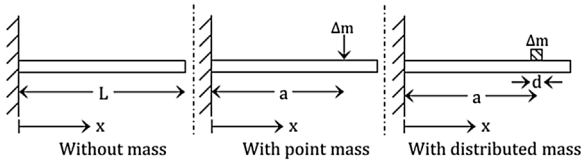

Fig. 3. Schematic representation of a cantilevered beam in three different configurations.

Please cite this article in press as: P. Gupta, et al., Evaluating tool point dynamics using output-only modal analysis with mass-change methods, NULL (2020), https://doi.org/10.1016/j.cirpj.2020.06.001

Eq. (13) can be modified for the case of the beam with a point mass, Δm, added at some distance 'a' from the clamped end, to become:

$$\rho A\frac{\delta^2 w}{\delta t^2}+EI\frac{\delta^4 w}{\delta x^4}=-\Delta m\frac{\delta^2 w}{\delta t^2}\delta(x-a), \tag{14}$$

wherein $\delta(.)$ is the Dirac-delta function. The clamped and free boundary conditions are the same as listed in Eq. (13). Due to the addition of the point mass, the compatibility equations ensuring continuity in the beam around the interface where the mass is added are:

$$\begin{aligned} &w(a)^-=w(a)^+;\\ &w'(a)^-=w'(a)^+;\\ &w''(a)^-=w''(a)^+;\\ &EIw'''(a)^+-EIw'''(a)^-=-\Delta m\ddot{w}(a), \end{aligned} \tag{15}$$

wherein, the superscripts, '−' and '+' denote the position slightly before and slightly after the interfacial point, respectively, and ".." in Eq. (15) denotes the double derivative with respect to time, t.

For the case of the beam with a distributed mass, we assume that the contact between the beam and the added mass is rigid. To simplify the analysis, we also assume that the mass addition poses no change in the area moment of inertia, I, and contributes only towards the total mass of the beam at the location of mass addition. The governing equation of motion for the beam with this distributed mass is:

$$\rho A\frac{\delta^2 w}{\delta t^2}+EI\frac{\delta^4 w}{\delta x^4}=-\Delta m\frac{\delta^2 w}{\delta t^2}\left[H\left(x-a-\frac{d}{2}\right)-H\left(x-a+\frac{d}{2}\right)\right], \tag{16}$$

wherein $H(.)$ is a Heaviside-step function. The clamped and free boundary conditions remain the same as in Eq. (13). Due to the addition of the distributed mass, the compatibility conditions ensuring continuity between the added mass and the beam for the region just before and after the region of the added mass are:

$$\begin{aligned} &w(a-d/2)^-=w(a-d/2)^+;\quad w(a+d/2)^-=w(a+d/2)^+;\\ &w'(a-d/2)^-=w'(a-d/2)^+;\quad w'(a+d/2)^-=w'(a+d/2)^+;\\ &w''(a-d/2)^-=w''(a-d/2)^+;\quad w''(a+d/2)^-=w''(a+d/2)^+;\\ &w'''(a-d/2)^-=w'''(a-d/2)^+;\quad w'''(a+d/2)^-=w'''(a+d/2)^+, \end{aligned} \tag{17}$$

wherein, as before, the superscripts, '−' and '+' denote the positions slightly before and slightly after interfacial points. Unlike the point mass case, in which, there was only one interface, and hence only four compatibility conditions, for this distributed mass case, there are two interfaces (before and after the mass), and hence there are eight conditions as listed in Eq. (17).

The modal solution to all three equations of motion, i.e., for Eqs. (13), (14), and (16), can be shown to be [43]:

$$\begin{aligned} &w(x,t)=\phi(x)h(t),\\ &\phi_k(x)=A_k\cos\beta_k x+B_k\cosh\beta_k x+C_k\sin\beta_k x+D_k\sinh\beta_k x,\\ &\omega=\beta_k^2\sqrt{E_kI_k/\rho_kA_k}\quad \text{where } k=1 \text{ to } N, \end{aligned} \tag{18}$$

wherein $\phi(x)$ and ω represents the mode shape, and natural frequency of the system, respectively, $h(t)$ represents the time component of the displacement and N represents the total number of segments in which the beam was divided into. A_k, B_k, C_k, and D_k in Eq. (18) can be found from the substitution of the appropriate compatibility criteria and boundary conditions. For example, for the case of the simple cantilevered beam, there is only one segment i.e. $N=1$ in Eq. (18). The four boundary conditions listed in Eq. (13) when substituted in the mode shape expression in Eq. (18) results in a transcendental equation in β with infinite solutions. In the domain of $\mathbb{R}^+$, the first solution corresponds to the first mode; the second solution corresponds to the second mode, and so on.

The solution to the cantilevered beam with a point mass was obtained by modelling the segments before and after the point mass separately, i.e. $N=2$ in Eq. (18). Hence the eight unknowns that need to be found (four unknowns for the segment to the left of the point mass, and four more unknowns for the segment to the right of the point mass), are obtained simultaneously by satisfying the four boundary conditions listed in Eq. (13) along with satisfying the four compatibility conditions in Eq. (15). As was done for the case of the simple cantilevered beam, solution to the resultant transcendental equation in β for this case too results in different modes.

Similar solution procedures are followed for the case of the beam with the distributed mass. In the distributed mass case, the beam is modelled in three segments ($N=3$), i.e., a segment just to the left of the added distributed mass, the segment with the distributed mass, and another segment just to the right of the added distributed mass. The twelve unknowns in the mode shape expression in Eq. (18) are obtained by using the eight compatibility conditions of Eq. (17) along with the four boundary conditions as listed in Eq. (13). The resulting transcendental equation in β was then used to determine the natural frequencies and mode shapes.

To demonstrate how the scaled (mass-normalized) and unscaled shapes are obtained from Eq. (18), consider the case of the cantilevered beam without any added mass. For this case, the mode shape from Eq. (18) will reduce to:

$$\phi_1(x)=A_1\cos\beta_1 x+B_1\cosh\beta_1 x+C_1\sin\beta_1 x+D_1\sinh\beta_1 x. \tag{19}$$

Eq. (19) has five unknowns – A_1, B_1, C_1, D_1, and β_1. Applying the boundary conditions given in Eq. (13), results in a transcendental equation in β_1 to determine the natural frequency:

$$1+\cos\beta L\cosh\beta L=0, \tag{20}$$

and, solving B_1, C_1, and D_1 in terms of A_1 results in:

$$\phi(x)=A_1(\cos\beta x+\gamma_1\cosh\beta x+\gamma_2\sin\beta x+\gamma_3\sinh\beta x), \tag{21}$$

wherein γ_1, γ_2, γ_3 relate A_1 to B_1, C_1, and D_1, and A_1 in turn is obtained from the mass-normalization condition of [43]:

$$\int_0^L m_m\phi^2(x)dx=1, \tag{22}$$

wherein m_m is the mass per unit length. Above analysis demonstrates the procedure to obtain the mass-normalized mode shapes. If, instead, the unscaled mode shapes are desired to be found (these are necessary for computing the necessary scaling factor), instead of obtaining A_1 from the mass-normalizing condition of Eq. (22), Eq. (21) can be left unscaled as:

$$\psi(x)=\cos\beta x+\gamma_1\cosh\beta x+\gamma_2\sin\beta x+\gamma_3\sinh\beta x, \tag{23}$$

wherein $\psi(x)$ represents the unscaled shape. Similar procedures as outlined above were adopted to find the (un)scaled mode shapes for the cantilevered beams with a point mass and with a distributed mass.

Having described the analytical cantilever beam model with the added point mass and the distributed mass and having discussed methods of solution for these models, the models are used to guide the selection of the size of the mass to be added and also to decide where the added mass is to be located such as to minimize the error in the scaled eigenvector – as discussed next. Error analysis for different scaling methods is also presented next. The sensitivity of scaling to errors in estimations of natural frequencies is also discussed. However, before proceeding with the error analysis, change in modal parameters due to the added mass is analyzed and discussed.

Change in modal parameters due to mass additions

The underlying assumption in mass-change methods is that with an additional mass added to the system of interest, there is an

Please cite this article in press as: P. Gupta, et al., Evaluating tool point dynamics using output-only modal analysis with mass-change methods, NULL (2020), https://doi.org/10.1016/j.cirpj.2020.06.001

insignificant change in the mode shape and that there is a noticeable shift in the natural frequency between the original and mass-modified system. The analytical model presented above is used to investigate the validity of this assumption. For the case of the cantilever beam with a distributed mass, the amount of mass is varied, and the absolute change (Δ) in the eigenvector at the tool point and the natural frequency between the original and mass-modified system is evaluated and is shown in Fig. 4. Results in Fig. 4 are obtained with beam parameters as listed in Table 1, and assuming that the added mass is kept at '$a = 230$ mm'. Results in Fig. 4 are reported only for the first mode, and the added mass is reported as a function of the modal mass of the first mode of the cantilever beam.

It is evident from Fig. 4 that an increase in the added mass causes a larger change in the natural frequency between the original and the mass-modified system than the change in the eigenvector between the two systems. It is also clear that the change in the eigenvectors is not insignificant – a 20% mass addition results in a ~17% change in the eigenvector. Hence, even though the mass-change methods presuppose that the change in the eigenvector between the original and mass-modified systems must remain negligible, and since the change is not negligible, it becomes crucial to systematically characterize the error in the estimation of the scaled eigenvectors with a change in the added mass. This error analysis is discussed next.

Error in the estimation of the mass-normalized eigenvectors

At first, for a fixed added mass, error in the estimation of the mass-normalized eigenvector at the free end for the two different methods to add the mass, i.e., a point mass, and a distributed mass, is characterized. We define the absolute error in the estimation of the mass-normalized eigenvector as:

$$e_\phi = \left| \frac{\phi - \alpha\psi}{\phi} \right|, \tag{24}$$

wherein ϕ is the true mass-normalized eigenvector at the free end, ψ is the unscaled eigenvector also at the free end, and α, the scaling factor is estimated from Eq. (12). Since only a single mass is added to the system, Eq. (12) reduces to: $\alpha^2 = \frac{\omega^2 - \hat{\omega}^2}{\hat{\omega}^2}\left(\psi^T \Delta m \psi\right)$, wherein Δm is the scalar mass addition. Since the scaling factor can be evaluated from eigenvectors estimated at the location of mass addition and also from the eigenvectors estimated at the free end, even when the mass is added elsewhere, sensitivity of e_ϕ to the two methods of scaling is also investigated herein.

For an added mass of 10% of the modal mass of the first mode of the cantilever, the error estimated with α obtained at the location of mass addition and at the free end is shown in Fig. 5 for both methods of adding the mass, i.e., the point mass, and the distributed mass. Fig. 5 reports errors as they change with the location of the added mass, and hence the abscissa represents a normalized length.

As is evident from Fig. 5, the errors change with the location, and the type of the added mass. For the case of the scaling factor obtained by using the eigenvectors obtained at the location of the added mass, the error profile for the estimation of the mass-normalized eigenvector at the free end is different for the case of the point and distributed mass – see Fig. 5(a) and (c). However, for the case of the scaling factor obtained by using the eigenvectors at the free end, the error profile for both methods of adding the mass are the same – see Fig. 5(b) and (d).

From Fig. 5(a), i.e., for the point mass case, with α obtained from using the eigenvectors evaluated at the location of the added mass, it appears that the error increases as the mass is placed towards the free end and that the error is minimum when the point mass is placed at '$a/L = 0.8$'. The error for this case also appears to reduce as the mass is moved towards the clamped end. Nevertheless, the error in the estimate of the mass-normalized eigenvector remains less than 0.5% irrespective of where the point mass is placed. Since in practice, it is not possible to place a point mass on the tool, the error profile for the distributed mass case is thought to be more useful to guide where the mass should be placed. As is evident from Fig. 5(c), for the distributed mass case with the scaling factor evaluated using the eigenvectors at the location of the added mass, e_ϕ reduces in an exponential manner as the mass is moved to the free end. And, as is evident from Fig. 5(d) for the distributed mass case with α obtained from using the eigenvectors at the free end, e_ϕ appears to reduce quadratically as the mass is moved from the clamped end to the free end. Even though this trend is similar for the case of adding a point mass (see Fig. 5(b)), since the distributed method of adding mass is more realistic, all subsequent investigations in this paper assume the added mass to be distributed in nature.

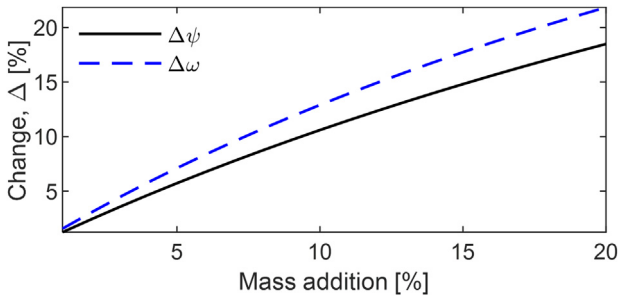

Fig. 4. Change in the eigenvector and the natural frequency with an increase in the added mass.

Table 1
Material parameters of the cantilever beam with distributed mass.

Radius, r	12.5 mm
Young's modulus, E	200 GPa
Length, L	250 mm
Density, ρ	7800 kg/m^3
Mass length, d	20 mm

Since the analysis in Fig. 5 is limited to only one mode, and to the case of adding only a fixed added mass, expanded analysis for two modes and with changing the amount of the added mass is shown in Fig. 6, in which the error, e_ϕ is represented by the colour-bar. Fig. 6 also schematically shows the mode shapes for the first two bending modes of the cantilever beam. The results observed for the error estimated with α obtained from using eigenvectors evaluated at the location of mass addition, and for α obtained from using eigenvectors evaluated at the free end are different but the trend is similar. As is evident from Fig. 6, for the first mode, the error is lowest around the free end whereas, in the case of the second mode, the lowest error is around the point of maximum deflection corresponding to the mode shape of the second modal frequency. It is also evident that the error increases around the location where the mode shape experiences zero deflection. This suggests that for a low e_ϕ, the mass to be added should be placed around the region of maximum deflection for that mode, and not near or at any nodal points. This observation is in line with the claim made in [37], for which we present reasoned confirmation.

Observations in Fig. 6 can be explained by substituting Eq. (12) in Eq. (24), which results in:

$$e_\phi = \left| 1 - \frac{\psi_T}{\phi_T \psi_a} \sqrt{\frac{\omega^2 - \hat{\omega}^2}{\hat{\omega}^2}} \Delta m \right|, \tag{25}$$

Please cite this article in press as: P. Gupta, et al., Evaluating tool point dynamics using output-only modal analysis with mass-change methods, NULL (2020), https://doi.org/10.1016/j.cirpj.2020.06.001

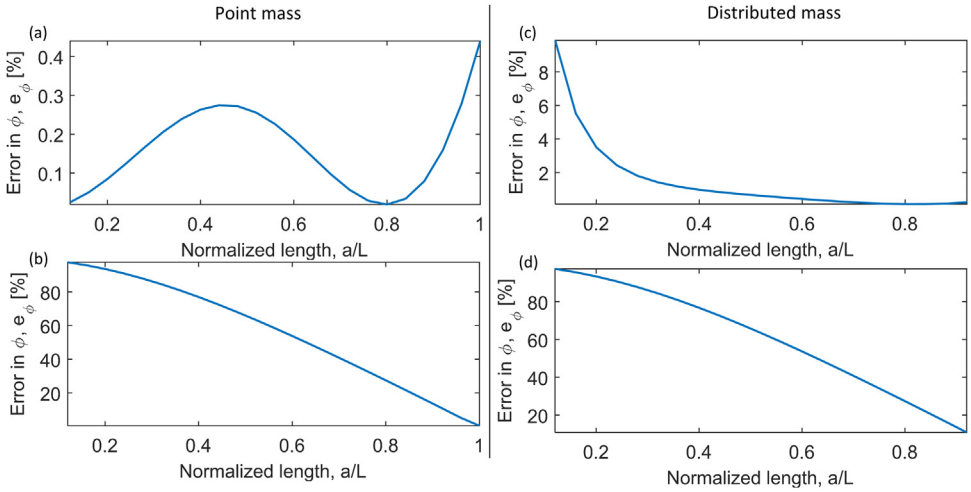

Fig. 5. Error in estimating mass-normalized eigenvector for two different methods to add the mass, i.e., for a point mass and a distributed mass being influenced by the location of the added mass, and method of scaling. (a) e_ϕ for the point mass case with α obtained from using the eigenvectors evaluated at the location of the added mass, (b) e_ϕ for the point mass case with α obtained from using the eigenvectors evaluated at the free end, (c) e_ϕ for the distributed mass case with α obtained from using the eigenvectors evaluated at the location of the added mass, (d) e_ϕ for the distributed mass case with α obtained from using the eigenvectors evaluated at the free end.

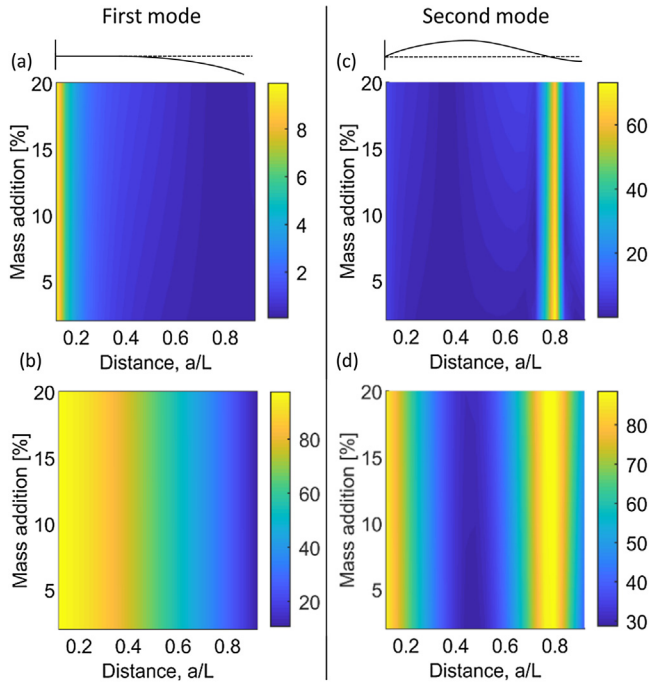

Fig. 6. Error in estimating mass-normalized eigenvectors for the first and second mode being influenced by the location of the added mass, and method of scaling. (a) e_ϕ for the first mode with α obtained from using the eigenvectors evaluated at the location of the added mass, (b) e_ϕ for the first mode with α obtained from using the eigenvectors evaluated at the free end, (c) e_ϕ for the second mode with α obtained from using the eigenvectors evaluated at the location of the added mass, (d) e_ϕ for the second mode with α obtained from using the eigenvectors evaluated at the free end.

wherein, ψ_T and ϕ_T are evaluated at the tool tip which are constant for a particular beam whereas ψ_a is the unscaled eigenvector as a function of distance 'a' from the clamped end. Clearly, Eq. (25) suggests that e_ϕ is a function of the mode shape estimate and that the error e_ϕ increases at the nodal point of the mode. It is also evident that e_ϕ is minimum for the eigenvector ψ_a estimated at the point of its maximum deflection, i.e., at the anti-node. Furthermore, Eq. (25) also suggests that the error e_ϕ becomes independent of the initial scaling in the unscaled eigenvector as the arbitrary scalar scaling factor multiplying ψ_T and ψ_a will cancel out. This property is useful in the sense that during experimentation, even if changing levels of input excitation will proportionally scale the eigenvector, the mass-normalized mode shape estimate, ϕ, remains independent of how ψ might scale.

From Figs. 5 and 6 we hence conclude that e_ϕ increases with increase in mass addition. To correctly estimate the mass-normalized eigenvector corresponding to a particular mode, Fig. 6 suggests that the mass to be added should be placed as close as possible to an anti-node and far from a nodal point for that mode of interest. Moreover, since Eq. (12) assumes the mode shape does not change with added mass, if Eq. (12) is 'strictly' valid, then, the error in the scaling factor simply scales by ψ_T/ψ_a if the mass was placed at distance 'a' from the clamped end instead of placing at the free end. However, since the mode shape *does* change with the amount and location of the added mass (see Figs. 4–6), Eq. (12) is an approximation, and given the influence of several intrinsically coupled factors on the error in the scaled mode shape, viz. the unscaled mode shape value at the location of the added mass, the shift in the frequency (which in turn depends on the location of the added mass), and the validity of Eq. (12) vis-a-vis the assumption of "negligible change in mode shape" (which again depends on the location of the added mass), the only tangible way of finding the optimal location of the added mass is through the numerical simulations presented above. These simulation results are supported by experimental validations discussed subsequently, after also discussing errors due to uncertainties in estimations of the natural frequencies.

Error due to uncertainty in the estimation of natural frequency

Another potential source of error is the error in the estimation of the scaling factor, α due to uncertainty in the measurement of natural frequency, ω. Uncertainties in estimation of natural frequencies are usual in experimental procedures [4], and hence to evaluate this error, Eq. (12) can be rewritten as:

$$\alpha^2 = \frac{\eta^2 - 1}{\psi^{\mathrm{T}} \Delta \mathbf{M} \psi}, \tag{26}$$

wherein $\eta = \omega/\hat{\omega}$. Furthermore, the error in the scaling factor due to error in the estimation of the natural frequency, ω can be

represented as [40]:

$$e_\omega = \frac{\delta\alpha}{\alpha} = \frac{\eta^2}{\eta^2 - 1}\frac{\delta\eta}{\eta}. \quad (27)$$

Assuming the error in η to be 0.1% [40], the error in the estimation of the scaling factor, α for different levels of the added distributed mass is evaluated and is shown in Fig. 7. The analysis herein is limited to the first mode.

As is evident from Fig. 7, the error in the estimation of the scaling factor, α due to uncertainty in the measurement of natural frequency, ω reduces with an increase in the amount of mass added to the system. Since uncertainties in correctly estimating the natural frequencies from experiments will remain present, this analysis shows that an increase in the added mass will reduce the potential error in the estimation of the scaling factor in the presence of uncertainties in ω. However, since an increase in the distributed mass causes a perceptible shift in the eigenvector – see Figs. 4 and 6, which in turn may result in other errors, increasing the mass to be added simply to account for errors in the estimates of the scaling factor due to natural frequency is not recommended.

Having systematically characterized the errors in the estimation of the mass-normalized eigenvector as well as the errors due to potential uncertainties in the estimates of the natural frequency, we also discuss below how the error in the eigenvector estimate is also governed by the choice of the formulation for the scaling factor.

Error in the estimate of the mass-normalized eigenvector being influenced by choice of the scaling factor

Though the scaling factor used in the above analysis was derived and presented in Eq. (12), other studies have made approximations [33], and yet others have presented alternate formulations for the scaling factor, and also expanded the scaling factors for more complex systems [37]. Since the choice of the scaling factor has bearing over the error in the estimate of the mass-normalized eigenvector, we present a comparative error analysis using different scaling factors that have been reported in the literature. The commonly used scaling factors are listed in Table 2, and the error in the estimation of the mass-normalized eigenvector, e_ϕ using the different scaling factors are evaluated for the first mode only and shown in Fig. 8. For this analysis, the distributed mass is assumed to be placed at a distance of 20 mm from the free end.

The first expression listed in Table 2, i.e., α_1 was given in [33] and involved an approximation of $\omega + \hat{\omega} \approx 2\hat{\omega}$. The remaining three were deduced in [37]. The second and fourth expressions, i.e., α_2 and α_4 differ only in terms of choice of unscaled eigenvector considered to evaluate the scaling factor, whereas the third expression, i.e., α_3 involves an expression evaluated from the mean of both the eigenvectors taken one at a time. The fourth expression is the same as derived in Eq. (12).

As is evident from Fig. 8, the choice of scaling factor significantly influences the error in the estimation of the mass-normalized eigenvector. The error in the estimation of the mass-normalized eigenvector increases for all the scaling factors with an increase in the added mass. Even though α_2 differs from α_4 only in its use of $\hat{\psi}$ in the denominator instead of ψ, its (α_2) use results in far greater errors than the use of α_4. Errors with α_2 are greater than those with α_4 mainly because of the mode shapes before and after the mass addition not remaining the same – see Fig. 4. From Fig. 4, it is evident that the difference between ψ and $\hat{\psi}$ is not negligible, and this difference between ψ and $\hat{\psi}$ translates to the difference observed between α_2 and α_4. Seeing that the formulation for α_4 reported in [37] is the same as that derived herein, for all further analysis we use the formulation for the scaling factor that is derived herein, i.e., the formulation described in Eq. (12).

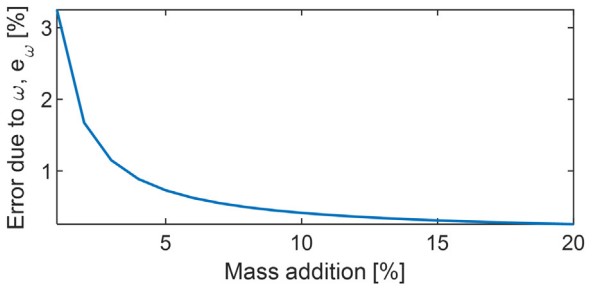

Fig. 7. Error due to uncertainty in the estimation of natural frequency, changing with added mass.

Table 2
Different formulations for scaling factor, α.

$\alpha_1 = \sqrt{\frac{2(\omega-\hat{\omega})}{\hat{\omega}\psi^{\mathrm{T}}[\Delta\mathbf{M}]\psi}}$	[33]
$\alpha_2 = \sqrt{\frac{\omega^2-\hat{\omega}^2}{\hat{\omega}^2}\psi^{\mathrm{T}}[\Delta\mathbf{M}]\hat{\psi}}$	[37]
$\alpha_3 = \frac{\sqrt{\frac{\omega^2-\hat{\omega}^2}{\hat{\omega}^2}\psi^{\mathrm{T}}[\Delta\mathbf{M}]\psi} + \sqrt{\frac{\omega^2-\hat{\omega}^2}{\hat{\omega}^2}\hat{\psi}^{\mathrm{T}}[\Delta\mathbf{M}]\hat{\psi}}}{2}$	[37]
$\alpha_4 = \sqrt{\frac{\omega^2-\hat{\omega}^2}{\hat{\omega}^2}\psi^{\mathrm{T}}[\Delta\mathbf{M}]\psi}$	[37]

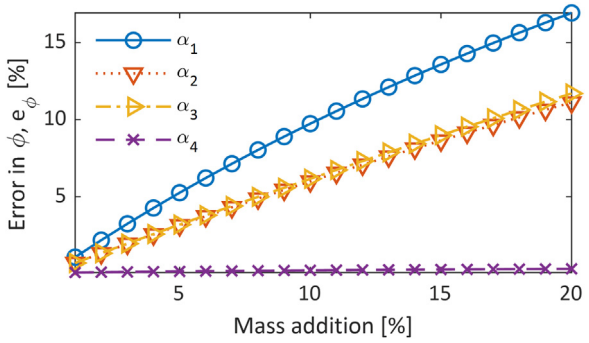

Fig. 8. Error in eigenvector estimate corresponding to different formulations of α.

Having presented an analytical model to guide the selection of the size of the mass to be added along with determining *where* to add that mass based on systematic error analysis, we first present experimental validation of the proposed mass-change methods on a simple cantilevered beam. Subsequently, we present the use of output-only mass-change methods to evaluate cutting tool point dynamics.

Preliminary experimental validation of the proposed mass-change method

This section presents experiments to validate the proposed mass-change method. Since a mass can be added to the test object in several ways, we investigate four different methods to add mass to a cantilevered beam – that is the test object in this preliminary experimental validation. The primary requirement for adding a mass to the test object is that the added mass must not have any relative motion to the test object, and hence it must be secured rigidly.

Please cite this article in press as: P. Gupta, et al., Evaluating tool point dynamics using output-only modal analysis with mass-change methods, NULL (2020), https://doi.org/10.1016/j.cirpj.2020.06.001

The four different types of masses added are shown in Fig. 9 and include the use of molybdenum piece that was stud mounted on to the beam, a magnet, a piece of clay, and a pair of aluminium strap clamps. All four types of the mass to be added weighed 42.5 ± 1 g. This weight was selected such that the added mass is 15% of the modal mass corresponding to the fundamental mode. This level of a mass addition of 15% was also done in order to observe a notable frequency shift between the original system and the mass-modified system. Moreover, pilot experiments with this weight of the mass showed frequency shifts greater than 1% for the mass placed and roved over 60% of the length of the cantilever beam. This was necessary to evaluate the errors in the estimation of the mass-normalized eigenvectors by varying the position of the mass to be added on the beam.

The cantilever beam selected as the test object was made of mild steel. The beam had a diameter of 25 mm and an overhang of 240 mm, and it was clamped in a compression holder – as shown in Fig. 10. Fig. 10 also shows the four different mass types mounted on the free end of the beam. In order to investigate experimentally how the dynamics change with a change in the position of the added mass, the mass was roved from a distance of 7.5 mm and up to a distance of 140 mm from the free end. Placing the mass beyond 140 mm was observed to result in a frequency shift of less than 1% – which was thought to be inadequate for correctly estimating the scaling factor.

Output-only analysis was carried out for experiments that were performed without the mass and with different types of masses placed at different locations along the beam. Since these preliminary experiments are to guide the evaluation of tool point dynamics, all experiments herein involved impacting near the free end and measuring the response at the free end. Though a modal hammer was used to excite the beam, the input remained unmeasured for the output-only analysis. The response was measured using a single axis accelerometer. All data was sampled at 25.6 kHz and the data was acquired using CutPro®'s data acquisition module [44]. The ERA was used to estimate the natural frequencies and unscaled mode shapes for experiments with and without the added mass. The scaling factor in Eq. (12) was then used to estimate the mass-normalized mode shape.

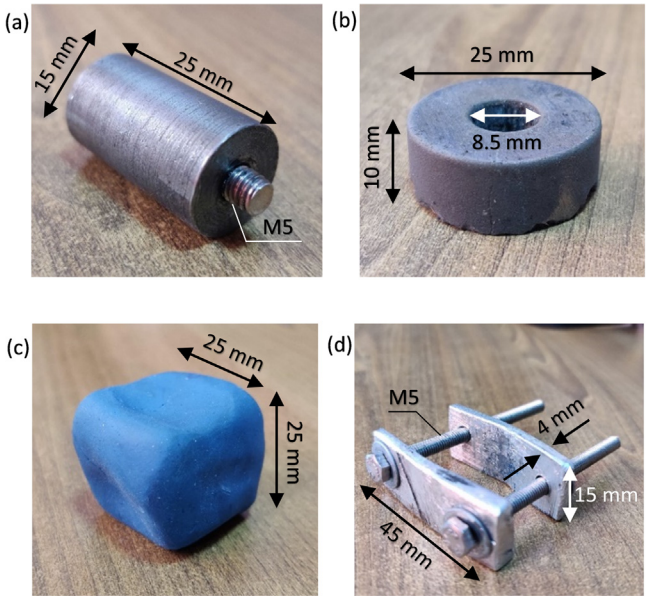

Fig. 9. Four different types of masses added to the primary test object, (a) molybdenum piece that is stud mounted, (b) magnet, (c) clay, (d) aluminium side clamps.

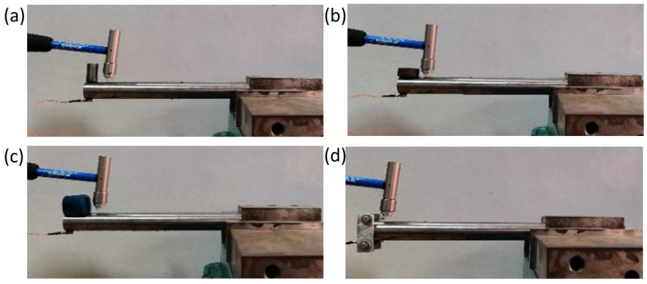

Fig. 10. Experimental setups with four different methods to add the mass on the cantilever beam, (a) stud mounted, (b) magnet, (c) clay, (d) side clamps.

The fundamental mode of the cantilever beam without any added mass was estimated to be 263.2 Hz, and the unscaled eigenvector at the free end of the beam was estimated to be 7.91 from the ERA analysis. Separate experimental modal analysis was also carried out for the beam without any added mass, in which the input and output were both measured using CutPro®'s data acquisition module and the modal parameters were extracted using CutPro®'s modal analysis module [44], from which the mass-normalized eigenvector was found to be 2.05. The error in the estimate of the mass-normalized eigenvector using the output-only mass-change method is benchmarked against this value. The results obtained with the four different ways to add the mass along different sections of the beam are summarized in Table 3 and Fig. 11.

As is evident from Table 3, as the mass is moved away from the free end, the natural frequency of the beam increases and tends towards the natural frequency estimate of the original beam without any additional mass placed on it. This is true for all four methods to add the mass. Also evident from Table 3 is that as all four types of the added mass are moved away from the free end, the scaling factor reduces, and the estimated mass-normalized eigenvector (estimated based on the output-only mass-change method) starts to deviate considerably from the mass-normalized eigenvector obtained from the experimental modal analysis procedure. These trends are plotted in Fig. 11, which confirms that as the added mass is moved towards the free end, i.e., towards the anti-node for the fundamental mode, the error in the estimate of the mass-normalized eigenvector reduces. This is consistent with the analytical model-based observations reported in Figs. 5(b) and 6(b) – thus validating the proposed output-only mass-change method. Though experimental validation of the proposed mass change method was presented herein only for the case of the scaling factor evaluated from eigenvectors estimated at the free end, even when the mass is added elsewhere, similar validation

Table 3
Parameters obtained for a cantilever beam for different mass addition techniques.

		Distance from the free end [mm]							
		7.5	20	40	60	80	100	120	140
Screw	$\hat{f}_n$ [Hz]	244.5	246.7	250.3	252.7	255.3	257.4	259.5	260.9
	α	0.24	0.23	0.20	0.18	0.15	0.13	0.10	0.08
	ϕ_{est}	1.93	1.81	1.58	1.41	1.22	1.04	0.83	0.66
Magnet	$\hat{f}_n$ [Hz]	244.1	245.7	250.1	252.7	255.2	257.5	259.5	261.0
	α	0.25	0.24	0.20	0.18	0.16	0.13	0.11	0.08
	ϕ_{est}	1.96	1.87	1.59	1.41	1.23	1.03	0.83	0.64
Clay	$\hat{f}_n$ [Hz]	245.1	246.6	250.3	252.4	254.8	256.9	258.7	260.5
	α	0.24	0.23	0.20	0.18	0.16	0.14	0.12	0.09
	ϕ_{est}	1.90	1.81	1.58	1.44	1.26	1.08	0.91	0.71
Clamp	$\hat{f}_n$ [Hz]	245.0	247.2	250.6	253.4	255.5	257.7	259.6	260.9
	α	0.24	0.22	0.20	0.17	0.15	0.13	0.10	0.08
	ϕ_{est}	1.91	1.78	1.56	1.37	1.20	1.01	0.81	0.66

Please cite this article in press as: P. Gupta, et al., Evaluating tool point dynamics using output-only modal analysis with mass-change methods, NULL (2020), https://doi.org/10.1016/j.cirpj.2020.06.001

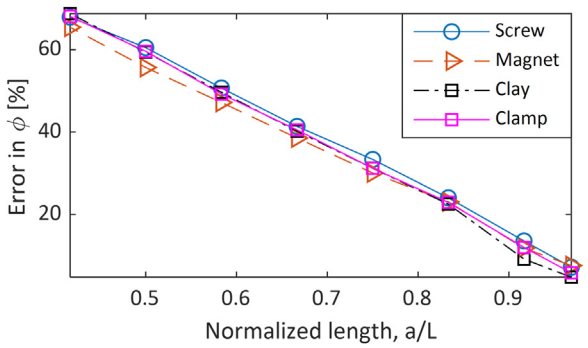

Fig. 11. Error in the estimation of mass-normalized eigenvectors for four different ways to add mass on a cantilever beam.

could also be shown for the scaling factor evaluated from eigenvectors estimated at the location of mass addition.

Seeing that the proposed output-only mass-change method holds promise, these methods are now used to guide the evaluation of tool point dynamics as is discussed next. Furthermore, Fig. 11 shows that there is no difference in the results obtained with the four different methods to add the mass. Even though the size of the four masses are different (see Fig. 9), because of their weight being similar, their different sizes do not appear to significantly influence the error in the estimation of mass-normalized eigenvectors – as is observable in Fig. 11. Since tools are generally made of carbide it is not possible to add a magnet to the tool, nor is it possible to stud mount anything on the tool, we hence prefer to use the aluminium strap clamps as a means to add a mass on the tool of interest. Moreover, the trend in the experimental results in Fig. 11 match the trend obtained with the analytical model for which results were shown in Fig. 5(d) – suggesting that the proposed analytical model can indeed be used to guide placement of the optimally sized mass on the tool to correctly estimate the tool point FRFs – as is discussed next.

Evaluating tool point dynamics using output-only mass-change methods

This section discusses the use of output-only mass-change methods to evaluate the tool point dynamics for two representative tools – a slender boring bar mounted on CNC lathe, and an end mill in a tool holder mounted on a CNC milling machine. For both tools, the output response for impact-based excitation was acquired using a single axis accelerometer mounted at the tool tip. For the output-only analysis, measurements were made with and without the added mass. Size and placement of the added mass were guided by the analytical models discussed above. All data was sampled at 25.6 kHz and acquired using CutPro®'s data acquisition module. Natural frequencies and unscaled mode shapes for the case of the tools with and without the added mass were evaluated using the ERA, and the scaling factor was then used to estimate the mass-normalized eigenvector correctly. Scaled shapes were contrasted with those obtained using traditional experimental modal analysis procedures in which the input and output were both measured and from which the modal parameters were evaluated using CutPro®'s modal analysis module.

The tool point frequency response functions for both tools were reconstructed from the extracted modal parameters for m modes of interest using:

$$h(\omega) = \sum_{j=1}^{m} \frac{\phi_j^2}{-\omega^2 + 2i\zeta_j\omega\omega_j + \omega_j^2}, \tag{28}$$

wherein ω_j, ζ_j and ϕ_j are the natural frequencies, damping ratios, and mass-normalized eigenvectors, respectively.

Results for the slender boring bar

A slender boring bar of 25 mm diameter and with a length-to-diameter ratio of 9 was mounted in a compression holder which in turn was mounted on a CNC machine. The experimental setup is shown in Fig. 12, which shows the accelerometer placed near the free end, and also shows the two different locations of the added mass to identify the dynamics of the first two bending modes. Placement of the added mass using aluminium strap clamps is guided by the analytical model that suggested adding the mass near the anti-node(s) for the mode(s) of interest. A mass of 42.5 g was added in both cases, and the analysis herein is limited to the *Y* direction only.

Following the procedure outlined above, the modal parameters obtained from the output-only mass-change analysis using the ERA are listed in Table 4. The added mass of 42.5 g corresponds to 15% of the modal mass of the fundamental mode and ~4% of the modal mass of the second mode. As is evident from Table 4, this mass-change resulted in a frequency shift of 8% for the fundamental mode and a 2% frequency shift for the second mode. There is also a perceptible change in the unscaled eigenvectors for the boring bar with and without the added mass. These frequency shifts and the unscaled eigenvector for the boring bar without the added mass were used to estimate the scaling factor and the mass-normalized eigenvector – that are also listed in Table 4.

To get a sense of the response signals with and without the added mass that were passed through the ERA to obtain the modal parameters of interest, Fig. 13 shows representative time and frequency plots of the response signals that were used to estimate the modal parameters of the first mode of the boring bar. Though the inputs were not used in the output-only mass-change method proposed herein, Fig. 13 includes a record of the measured input impulse force signals to demonstrate that the bandwidth excited spans the frequency range of interest. As is evident from Fig. 13, the bandwidth for both cases, i.e., for the case without the added mass, and for the case with the added mass, is the almost the same, being ~1.2 kHz – suggesting that all modes within this bandwidth should be identifiable. Furthermore, as is also evident from Fig. 13, even though the input force levels and the bandwidths for measurements with and without the mass are alike, the response for both cases is different. The maximum acceleration levels for the

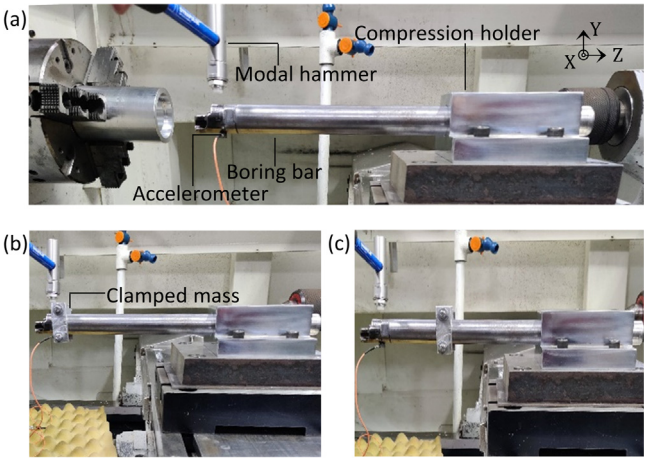

Fig. 12. Experimental setups to evaluate dynamics of a boring bar, (a) without any mass added, (b) mass added to evaluate the first mode, (c) mass added to evaluate the second mode.

Please cite this article in press as: P. Gupta, et al., Evaluating tool point dynamics using output-only modal analysis with mass-change methods, NULL (2020), https://doi.org/10.1016/j.cirpj.2020.06.001

Table 4
Modal parameters for the boring bar obtained from the output-only ERA and mass-change method.

		f_n [Hz]	$\psi; \hat{\psi}$	α	ϕ
1st mode	Without mass	361.3	17.17	0.11	1.98
	With mass	334.5	14.00		
2nd mode	Without mass	1920	12.45	0.078	0.97
	With mass	1882.4	7.304		

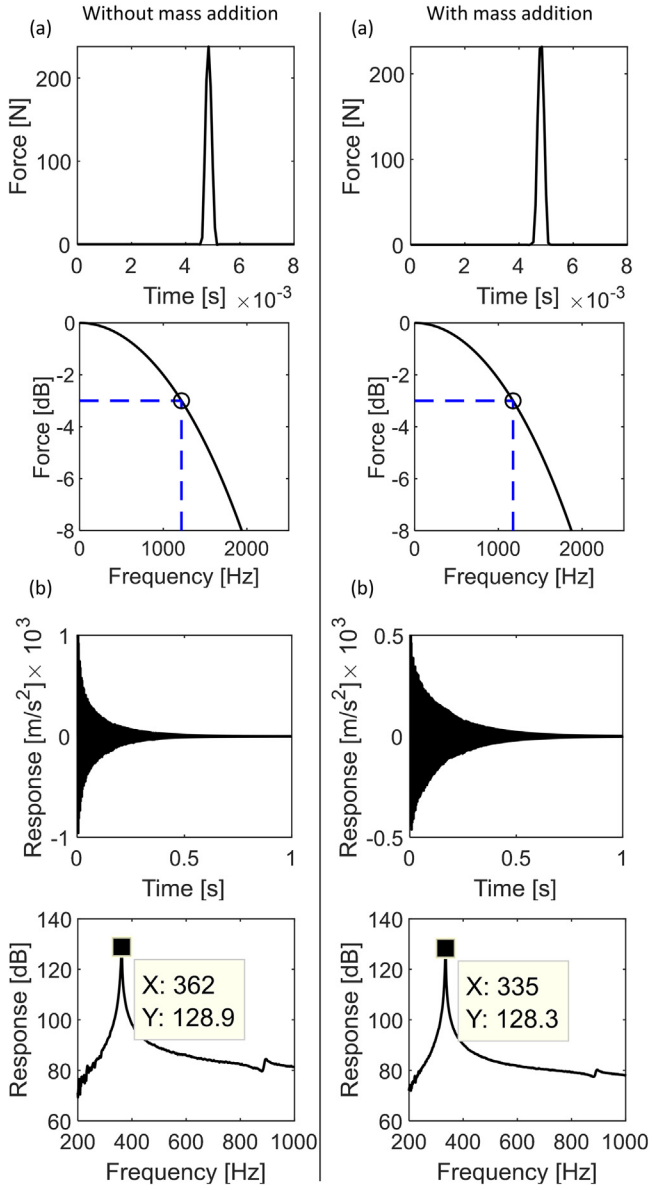

Fig. 13. Time and frequency plots of the signals that were used to estimate the modal parameters of the first mode of the boring bar. Left column corresponds to the case without the added mass, and the right column corresponds to the case with the added mass. (a) Impulse input force and its frequency spectra, and (b) Acceleration response and its frequency spectra.

response without the added mass reach $\pm\sim$1000 m/s^2, whereas for the case with the added mass, the maximum acceleration levels observed are $\pm\sim$500 m/s^2. Furthermore, the frequency spectra of the response signals further confirm that the strength of the output response with the added mass is slightly lesser than the case without the mass. Also evident from the frequency spectra is the reduction in the frequency of the dominant mode for the case of the added mass. The differences in the response and in their spectra shown in Fig. 13 are essential for estimating the scaling factor (see Eq. (12)) necessary to scale the eigenvector. Since the frequencies in the response spectra in Fig. 13 are evaluated from the Fourier transform, these are slightly different than those reported in Table 4 – which are output directly from the ERA.

The natural frequencies and damping ratio for the boring bar without the added mass and the mass-normalized eigenvectors obtained using the output-only mass-change method is compared in Table 5 with the modal parameters obtained using the traditional experimental modal analysis procedures. Furthermore, as is evident in Table 5, the damping and mass-normalized eigenvector obtained using the proposed output-only mass-change method are only slightly overestimated in contrast to the results from the traditional EMA procedures. These parameters are used to reconstruct the FRFs at the free end and those results are compared in Fig. 14, which also includes the measured FRF before modal curve-fitting. As is evident from Fig. 14, all three FRFs compare very well – further validating the proposed method and demonstrating how the method can be used to estimate the dynamics of tools with multiple modes.

Results for an end mill cutting tool

The proposed methods were also demonstrated on an end mill of 20 mm diameter mounted in a tool holder with an overhang of 85 mm – as shown in Fig. 15. The experimental setup in Fig. 15 shows the end mill with and without the added mass. Unlike for the case of the slender boring bar discussed above, the analysis herein is only limited to that for a single mode, since preliminary investigations showed the end mill's dynamics to be dominated by a single mode in the frequency range between 100 and 2000 Hz. The added mass of 42.5 g was placed at the anti-node which happens to be the tool tip. The accelerometer too, was mounted on the tool tip. Though the setup shown in Fig. 15 is for measuring the dynamics in the *X* direction, a similar setup (not shown) was also used to measure the end mill's dynamics in the *Y* direction.

Similar procedures as were followed for the boring bar were also followed herein, and the modal parameters obtained from the output-only mass-change analysis using the ERA are listed in Table 6.

The added mass of 42.5 g corresponds to 4–5% of the modal mass of the fundamental modes in the X and Y directions, respectively. As is evident from Table 6, this mass-change resulted in a frequency shift of ~2% for the fundamental modes in the *X* and *Y* directions. However, unlike the case for the boring bar, in the present case, there is a negligible change in the unscaled eigenvectors for the end mill with and without the added mass in either of the principal directions. As before, the frequency shifts, and the unscaled eigenvectors for the end mill without the added mass were used to estimate the scaling factor and the mass-normalized eigenvector – that are also listed in Table 6.

The mass-normalized eigenvector, damping ratio and the natural frequencies for the end mill without the added mass obtained with the output-only analysis are compared in Table 7 with modal parameters obtained using the traditional EMA

Table 5
Modal parameters for the boring bar obtained using the proposed output-only mass-method and the traditional EMA method.

	Proposed output-only mass-change method			EMA		
	f_n [Hz]	ζ [%]	ϕ	f_n [rad/s]	ζ [%]	ϕ
1st mode	361.3	0.46	1.98	362	0.42	1.93
2nd mode	1920	0.58	0.97	1918	0.50	0.88

Please cite this article in press as: P. Gupta, et al., Evaluating tool point dynamics using output-only modal analysis with mass-change methods, NULL (2020), https://doi.org/10.1016/j.cirpj.2020.06.001

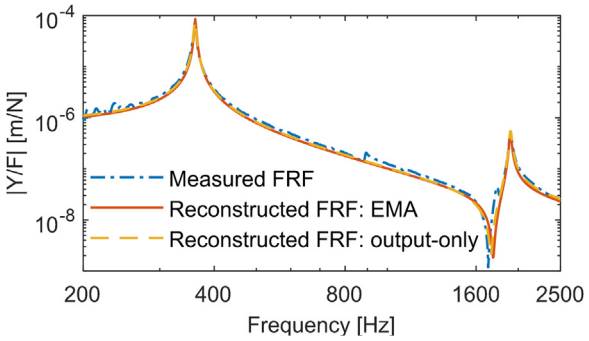

Fig. 14. Comparison of the measured FRF before modal curve-fitting with FRFs reconstructed with modal parameters extracted using the traditional EMA approach and with parameters obtained using the proposed output-only mass change method.

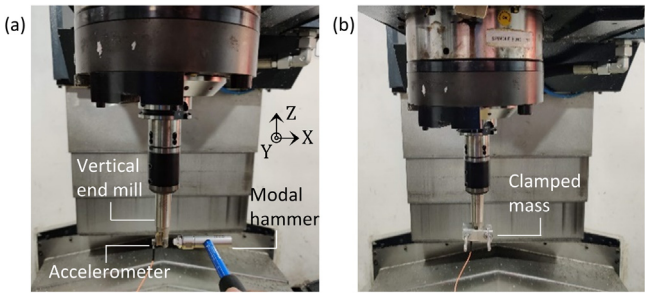

Fig. 15. Experimental setup to evaluate dynamics of an end mill, (a) without any mass added, (b) mass added to evaluate dynamics in the *X* direction.

Table 6
Modal parameters for the end mill obtained from the output-only ERA and mass-change method.

		f_n [Hz]	$\psi; \hat{\psi}$	α	ϕ
X	Without mass	637.2	6.89	0.14	0.94
	With mass	625.6	7.22		
Y	Without mass	656.4	8.19	0.13	1.09
	With mass	640.4	6.87		

Table 7
Modal parameters for the end mill obtained using the proposed output-only mass-method and the traditional EMA method.

	Proposed output-only mass-change method			EMA		
	ω_n [rad/s]	ζ [%]	ϕ	ω_n [rad/s]	ζ [%]	ϕ
X	$2\pi \cdot 637.2$	2.48	0.94	$2\pi \cdot 641$	2.47	1.00
Y	$2\pi \cdot 656.4$	1.95	1.09	$2\pi \cdot 655$	2.00	0.99

procedures, and as is evident, the modal parameters are in excellent agreement with each other. Since the modal parameters are in such close agreement, the FRFs reconstructed with these parameters that are contrasted in Fig. 16 are also naturally in good agreement. Fig. 16 also shows the measured FRFs before curve fitting, and the close agreement of the dominant mode in the measured FRF before curve fitting, and the FRFs reconstructed with modal parameters listed in Table 7 further confirms the ability of the proposed output-only mass-change methods to estimate tool point dynamics correctly.

Since methods presented herein were limited to evaluating the modal parameters of only the dominant mode(s), the other higher-frequency modes appearing in the measured FRFs were not paid heed to, nor were the lower-frequency structural modes, and as

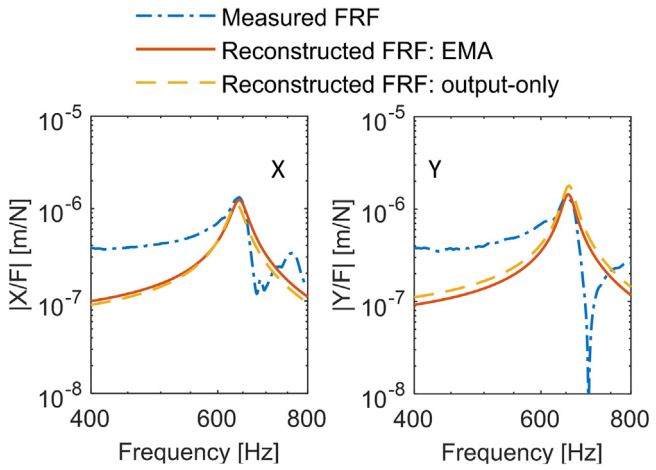

Fig. 16. Comparison of the measured FRFs before modal curve-fitting with FRFs reconstructed with modal parameters extracted using the traditional EMA approach and with parameters obtained using the proposed output-only mass change method. *X*-directional FRFs are shown on the left, and the *Y*-directional FRFs are shown on the right.

such, even if the dominant mode is captured well, modal truncation introduced errors are evident. These could be addressed by including low-and-high-frequency residuals, or the output only mass-change method could also be used to place potentially different masses at the anti-nodes of these low-and-high frequency modes to also extract their modal parameters. This would be like what was demonstrated for identifying the second bending mode of the slender boring bar. Since the modes of the end mill are reasonably well separated in the present analysis, different mass additions to extract the different modal parameters may prove feasible. However, for the more general case of extending the proposed output-only mass-change methods to evaluating the dynamics of machines with potentially closely spaced spindle and tool holder modes, if measurements were to be undertaken using only a single sensor, mode switching might go undetected, and the scaled mode shapes might be erroneous. Addressing these issues is difficult and remains largely unexplored. Though this is not part of the present scope of this paper, such questions can be explored in future studies.

Conclusions

This paper presented a new output-only mass-change method to estimate cutting tool point dynamics. Since output-only modal analysis methods result in the eigenvector estimates to be unscaled, we presented analytical models to guide the sizing and placement of the mass to be added on the tool such as to correctly estimate mass-normalized eigenvectors to be used in constructing tool point frequency response functions.

Analytical models include systematic characterization of errors in scaling the eigenvector and of errors due to uncertainties in the estimation of the natural frequencies. Analytical models also guide the appropriate use of scaling formulations. Analytical models suggest the mass to be added for scaling to be placed at/near the anti-node(s) for the mode(s) of interest. Since the analytical models include modelling the mass to be added in a distributed sense as opposed to considering the added mass to be a point mass – as was done by others before, the proposed model is thought to be more representative of the real case – in which any added mass will always be distributed. These analytical models were validated experimentally, and those results were used to guide the evaluation of cutting tool point dynamics using output-only mass-change methods.

Please cite this article in press as: P. Gupta, et al., Evaluating tool point dynamics using output-only modal analysis with mass-change methods, NULL (2020), https://doi.org/10.1016/j.cirpj.2020.06.001

Methods were demonstrated on two representative cutting tools – a slender boring bar mounted in a CNC lathe, and on an end mill mounted in a holder on a CNC milling machine. Modal parameters estimated with the proposed output-only mass-change methods were shown to compare well with modal parameters estimated using the traditional experimental modal analysis procedures. Since modal parameters compared well, tool point frequency response functions reconstructed using modal parameters that were estimated using the proposed methods were also found to be in good agreement with FRFs reconstructed using modal parameters obtained from traditional EMA procedures.

The main advantage of the proposed methods is thought to be the requirement of one less force transducer, and hence the proposed methods promise advantages from the industrial point-of-view. Moreover, the demonstrated success of using mass-change methods for evaluating tool point dynamics may pave the way for using mass-change methods in conjunction with operational modal analysis to identify the in-process dynamics of machine tools.

The proposed output-only mass-change methods need experiments to be conducted on tools with and without adding an additional mass, and as such the proposed methods need more experiments than the traditional experimental modal analysis procedures, and this is thought to be the main drawback of the proposed method. Furthermore, the proposed methods are more suitable for cantilevered tooling systems and remain untested for evaluating the dynamics of larger machine tool structural elements. Moreover, though the analysis presented herein was limited to the case of the modes identified being very well separated, how output-only mass-change methods might work for the case of the dynamics being dominated by closely spaced modes, such as for the case in milling machines with the spindle and tool holder modes being closely spaced, is largely unexplored, and can form part of future studies.

Declaration of competing interests

The authors declare that they have no known competing financial interests or personal relationships that could have appeared to influence the work reported in this paper.

Acknowledgments

This work was partially supported by the Government of India's Impacting Research Innovation and Technology (IMPRINT) initiative through project number IMPRINT 5509.

References

[1] Altintas, Y., 2004, Critical review of chatter vibration models for milling. Auton. Produktion, Springer: 39–60.
[2] Quintana, G., Ciurana, J., 2011, Chatter in machining processes: a review. Int J Mach Tools Manuf, 51:363–376. http://dx.doi.org/10.1016/j.ijmachtools.2011.01.001.
[3] Munoa, J., Beudaert, X., Dombovari, Z., Altintas, Y., Budak, E., Brecher, C., et al, 2016, Chatter suppression techniques in metal cutting. CIRP Ann – Manuf Technol, 65:785–808. http://dx.doi.org/10.1016/j.cirp.2016.06.004.
[4] Ewins, D.J., 2000, Modal testing: theory, practice and application, vol. 171.Res Stud Press LTD, Baldock, Hertfordshire, Engl. 415–37.
[5] Brincker, R., Ventura, C., 2015, Introduction to operational modal analysis. John Wiley & Sons.
[6] Zaghbani, I., Songmene, V., 2009, Estimation of machine-tool dynamic parameters during machining operation through operational modal analysis. Int J Mach Tools Manuf, 49:947–957.
[7] Özşahin, O., Budak, E., Özgüven, H.N., 2011, Investigating dynamics of machine tool spindles under operational conditions. Adv Mater Res, 223:610–621.
[8] Cai, H., Mao, X., Li, B., Luo, B., 2015, Estimation of FRFs of machine tools in output-only modal analysis. Int J Adv Manuf Technol, 77:117–130.
[9] Iglesias, A., Munoa, J., Ramírez, C., Ciurana, J., Dombóvári, Z., 2016, FRF estimation through sweep milling force excitation (SMFE). Proc CIRP, 46:504–507.
[10] Berthold, J., Kolouch, M., Wittstock, V., Putz, M., 2016, Broadband excitation of machine tools by cutting forces for performing operational modal analysis. MM Sci J, 1473–1481.
[11] Aguirre, G., Iglesias, A., Munoa, J., Astarloa, A., Ciurana, J., 2014, Real milling force based dynamic parameter extraction method. Int Conf Noise Vib Eng, .
[12] Liu, H., He, Y., Mao, X., Li, B., Liu, X., 2017, Effects of cutting conditions on excitation and dynamic stiffness in milling. Int J Adv Manuf Technol, 91:813–822.
[13] Powałka, B., Jemielniak, K., 2015, Stability analysis in milling of flexible parts based on operational modal analysis. CIRP J Manuf Sci Technol, 9:125–135.
[14] Peng, Y., Li, B., Mao, X., Liu, H., Qin, C., He, H., 2018, A method to obtain the in-process FRF of a machine tool based on operational modal analysis and experiment modal analysis. Int J Adv Manuf Technol, 95:3599–3607.
[15] Postel, M., Özsahin, O., Altintas, Y., 2018, High speed tooltip FRF predictions of arbitrary tool-holder combinations based on operational spindle identification. Int J Mach Tools Manuf, 129:48–60.
[16] Li, B., Cai, H., Mao, X., Huang, J., Luo, B., 2013, Estimation of CNC machine–tool dynamic parameters based on random cutting excitation through operational modal analysis. Int J Mach Tools Manuf, 71:26–40.
[17] Berthold, J., Kolouch, M., Wittstock, V., Putz, M., 2018, Identification of modal parameters of machine tools during cutting by operational modal analysis. Proc CIRP, 77:473–476.
[18] Maamar, A., Le, T.-P., Gagnol, V., Sabourin, L., 2019, Modal identification of a machine tool structure during machining operations. Int J Adv Manuf Technol, 102:253–264.
[19] Poddar, D., Shunmugam, M.S., 2019, Development of an automated modal extraction methodology through OMA by random cutting excitation of a legacy milling machine. Mech Syst Signal Process, 122:448–462.
[20] Cai, H., Luo, B., Mao, X., Gui, L., Song, B., Li, B., et al, 2015, A method for identification of machine-tool dynamics under machining. Proc CIRP, 31:502–507.
[21] Mao, X., Yan, R., Cai, H., Li, B., Luo, B., He, S., 2016, A complete methodology for identifying dynamics of heavy machine tool through operational modal analysis. Proc Inst Mech Eng Part B J Eng Manuf, 230:1406–1416.
[22] Berthold, J., Kolouch, M., Regel, J., Putz, M., 2019, Investigation of the dynamic behavior of machine tools during cutting by operational modal analysis. MM Sci J 2019, 3078–3085. http://dx.doi.org/10.17973/MMSJ.2019_11_2019054.
[23] Chan, Y.J., Huang, J.-W., 2018, Time-domain operational modal analysis in machine tools: optimal parameters and practical issues. Int J Precis Eng Manuf, 19:889–897.
[24] Li, B., Li, L., He, H., Mao, X., Jiang, X., Peng, Y., 2019, Research on modal analysis method of CNC machine tool based on operational impact excitation. Int J Adv Manuf Technol, 1–20.
[25] Suzuki, N., Kurata, Y., Kato, T., Hino, R., Shamoto, E., 2012, Identification of transfer function by inverse analysis of self-excited chatter vibration in milling operations. Precis Eng, 36:568–575.
[26] Özşahin, O., Budak, E., Özgüven, H.N., 2015, In-process tool point FRF identification under operational conditions using inverse stability solution. Int J Mach Tools Manuf, 89:64–73.
[27] Eynian, M., 2019, In-process identification of modal parameters using dimensionless relationships in milling chatter. Int J Mach Tools Manuf, 143:49–62.
[28] Kim, S., Ahmadi, K., 2019, Estimation of vibration stability in turning using operational modal analysis. Mech Syst Signal Process, 130:315–332.
[29] Ahmadi, K., Altintas, Y., 2014, Identification of machining process damping using output-only modal analysis. J Manuf Sci Eng, 136.
[30] Wan, M., Feng, J., Ma, Y.-C., Zhang, W.-H., 2017, Identification of milling process damping using operational modal analysis. Int J Mach Tools Manuf, 122:120–131.
[31] Mao, X., Luo, B., Li, B., Cai, H., Liu, H., Pen, F., 2014, An approach for measuring the FRF of machine tool structure without knowing any input force. Int J Mach Tools Manuf, 86:62–67.
[32] Ahmadi, K., 2018, Output-only modal analysis of micromilling systems. J Micro Nano-Manuf, 6.
[33] Parloo, E., Verboven, P., Guillaume, P., Van Overmeire, M., 2002, Sensitivity-based operational mode shape normalisation. Mech Syst Signal Process, 16:757–767. http://dx.doi.org/10.1006/mssp.2002.1498.
[34] Brincker, R., Andersen, P., 2003, A way of getting scaled mode shapes in output only modal testing. Int Modal Anal Conf – 3–6 February 2003, .
[35] Coppotelli, G., 2009, On the estimate of the FRFs from operational data. Mech Syst Signal Process, 23:288–299. http://dx.doi.org/10.1016/j.ymssp.2008.05.004.
[36] Bernal, D., 2011, A receptance based formulation for modal scaling using mass perturbations. Mech Syst Signal Process, 25:621–629. http://dx.doi.org/10.1016/j.ymssp.2010.08.004.
[37] López-Aenlle, M., Fernández, P., Brincker, R., Fernández-Canteli, A., 2010, Scaling-factor estimation using an optimized mass-change strategy. Mech Syst Signal Process, 24:1260–1273. http://dx.doi.org/10.1016/j.ymssp.2009.06.011.
[38] Behnam, M.R., Khatibi, M.M., Malekjafarian, A., 2018, An accurate estimation of frequency response functions in output-only measurements. Arch Appl Mech, 88:837–853.
[39] Khatibi, M.M., Ashory, M.R., Albooyeh, A.R., 2011, Optimum amount of additive mass in scaling of operational mode shapes. Struct Eng Mech, 39:733–750.

Please cite this article in press as: P. Gupta, et al., Evaluating tool point dynamics using output-only modal analysis with mass-change methods, NULL (2020), https://doi.org/10.1016/j.cirpj.2020.06.001

[40] Villa-García, L.M., 2015, Error analysis in obtaining scale factors with operational modal analysis and mass change. Rev Fac Ing Univ Antioquia, 202–210.
[41] Juang, J.N., Pappa, R.S., 1985, An eigensystem realization algorithm for modal parameter identification and model reduction. J Guid Control Dyn, 8:620–627. http://dx.doi.org/10.2514/3.20031.
[42] Mukhopadhyay, S., Luş, H., Betti, R., 2016, Structural identification with incomplete output-only data and independence of measured information for shear-type systems. Earthq Eng Struct Dyn, 45:273–296.
[43] Hagedorn, P., DasGupta, A., 2007, Vibrations and waves in continuous mechanical systems. Wiley Online Library.
[44] CUTPRO V11.2. Adv Mach Simul Softw ©MAL Inc.

Please cite this article in press as: P. Gupta, et al., Evaluating tool point dynamics using output-only modal analysis with mass-change methods, NULL (2020), https://doi.org/10.1016/j.cirpj.2020.06.001